White Light Electrophosphorescence from Polyfluorene-Based Light-Emitting Diodes: Utilization of Fluorenone Defects†

Xiong Gong, D. Moses,* and Alan J. Heeger‡

Center for Polymers and Organic Solids, University of California at Santa Barbara, Santa Barbara, California 93106

Steven Xiao

Organic Vision Inc., 3455 Isabelle, Brossard, Quebec, Canada J4R 2R2

Received: January 15, 2004; In Final Form: March 23, 2004

Poly(9,9-dioctylfluorene-*co*-fluorenone) with 1% fluorenone, (PFO−F(1%)), was synthesized as a model compound to investigate the optical and electrical effects of fluorenone defects in poly(9,9-dioctylfluoren-2,7-diyl), PFO. Photoluminescence (PL) and electroluminescence (EL) measurements demonstrate that PFO−F(1%) emits stable green light. PL and EL studies indicate that Förster energy transfer to and charge carrier trapping on fluorenone defects (with subsequent fluorenone emission) are responsible for the color degradation typically observed with the polyfluorenes. By utilization of "fluorenone defects" in PFO−fluorenone copolymers (PFO−F), white electrophosphorescent light-emitting diodes were fabricated. Polymer blends were spin-cast from solution containing PFO, PFO−F (1%), and tris[2,5-bis(9,9-dihexylfluoren-2-yl)pyridine-κ^2NC_3]iridium-(III), $Ir(HFP)_3$. The white emission turns on at approximately 5 V, with a luminance (L) of 6100 cd/m^2 at 17 V. The luminous efficiency is 3 cd/A at current density of 8.5 mA/cm^2 (L = 255 cd/m^2). The white light exhibits stable color coordinates and stable color temperature and has a high color rendering index.

Introduction

Semiconductoring (conjugated) polymers are of considerable importance as the active materials in emerging new technologies such as electronic and optical devices including polymeric light-emitting diodes (PLEDs), photodetectors, photovoltaic cells, sensors, field-effect transistors, and lasers.[1−6] Because of the opportunities associated with the use of PLEDs in display applications, the development of conjugated polymers that show efficient, stable blue, green, and red emission is an ongoing research effort.[7−11]

PLEDs which emit white light are of interest for use as backlights in high efficiency active matrix displays (with color filters) and because they might eventually be used for solid-state lighting.[1] In such applications, manufacturing costs will be a major issue. The fabrication of PLEDs by processing the active materials from solution promises to be much less expensive than that of OLEDs (based on small molecules) where the active layers require high-vacuum deposition. Several approaches have been used to generate white light from PLEDs and OLEDs.[10−16] However, the CIE (Commission Internationale d'Eclairage) coordinates depend on the performance of blue emitters, which have been reported to be unstable.[7−9]

Polyfluorenes (PFs), as efficient blue emitters, have emerged as an important class of conjugated polymers. They exhibit high photoluminescence (PL) efficiency, good charge-transport and thermal stability. In addition, their physical parameters can be varied through chemical modification and copolymerization.[7] Moreover, as host materials, the PFs enable full color (blue, green, and red) via energy transfer to longer wavelength emitters in blends with other conjugated polymers, phosphorescent dyes, and organometallic emitters.[17,18] Consequently, the PFs are interesting candidates as materials for use in the fabrication of PLEDs that emit white light. In such white emitting PLEDs, the PFs can function both as the host and as the blue emitter.

Typically, however, a low-energy (2.2−2.4 eV) green PL band appears in the emission from PFs over time and degrades the blue emission. A number of mechanisms were proposed for the origin of this low-energy emission.[15,19−25] Scherf and his colleagues[21−24] suggested that the green emission band originated from *keto* defects introduced either during synthesis or by photooxidation. Subsequently, we presented comprehensive evidence that the green emission band originates from *fluorenone defects* rather than from aggregation or excimer formation.[25] We demonstrated that *fluorenone defects* are generated by photooxidation and by thermal-oxidation and that the formation of *fluorenone defects* in the PFs is catalyzed by the low work function metals used as cathode materials in light emitting diodes.[25]

Having identified the role of fluorenone defects in the PFs, two opportunities emerge. First, one can stabilize the blue emission from PFs by excluding the formation of fluorenone defects. Alternatively, one can take advantage of the fluorenone defect for creating materials with stable green emission. We exploit both of these opportunities. An approach toward stabilization of the blue emission from polyfluorene-based PLEDs has been reported elsewhere.[25]

Poly(9,9-dioctylfluorene-*co*-fluorenone) with 1% fluorenone (PFO−F(1%)) was synthesized as a model compound to investigate the optical and electrical effects of fluorenone defects

† Part of the special issue "Alvin L. Kwiram Festschrift".

* Corresponding author. E-mail: moses@ipos.ucsb.edu. Fax: (805) 893-4755.

‡ Department of Physics and Materials Department, University of California at Santa Barbara, Santa Barbara, CA 93106.

10.1021/jp040027v CCC: $27.50
Published on Web 05/12/2004

CHART 1: Molecular Structures of PFO, PFO−F (1%), Fluorenone Derivative and Ir(HFP)$_3$

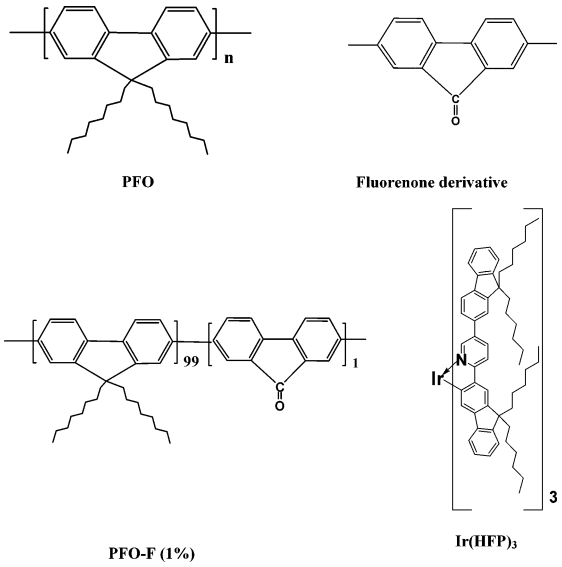

in poly(9,9-dioctylfluoren-2,7-diyl) (PFO). The PL and electroluminescence (EL) spectra demonstrated that PFO−F (1%) emits very stable green light. The spectroscopic and cyclic voltammetry studies on fluorene/fluorenone copolymers comprising 1% fluorenone demonstrate that efficient energy transfer and charge trapping cause the undesired spectral shifts observed in the PL and EL of PFO. White electrophosphorescent light-emitting diodes were fabricated by spin-casting polymer blends from solution containing PFO, PFO−F (1%), and tris[2,5-bis-(9,9-dihexylfluoren-2-yl)pyridine-$\kappa^2NC_{3'}$]iridium(III), Ir(HFP)$_3$. The CIE coordinates from observed white light are insensitive to the brightness of the emitted light and applied voltages.

Experimental Section

(1) Synthesis of Poly(9,9-dioctylfluorene-*co*-fluorenone) Copolymer (PFO−F (1%)).[16] A thoroughly dried three-neck flask (500 mL) was flushed with nitrogen and charged with 20 mL of dry *N*,*N*-dimethylformamide (DMF), 1 mL of 1,5-cyclooctadiene (COD, 7.3 mmol), 1.14 g of 2,2′-dipyridyl (7.3 mmol), and 2.0 g of bis(1,5-cyclooctadiene)nickel(0) (Ni(COD)$_2$, 7.3 mmol). The mixture was slowly heated to 70 °C and became deep purple in color. To this solution, a pre-degassed toluene solution containing 1.98 g of 9,9-dioctyl-2,7-dibromofluorene (3.6 mmol) and 0.013 g of 2,7-dibromo-9-fluorenone (0.036 mmol) was added. The resulting mixture was stirred for 72 h at 80 °C. The polymer was then precipitated with a mixture of methanol, acetone, and hydrochloric acid. After thorough cleaning, the polymer was dried in a vacuum at room temperature.

The synthesis and characterization of tris[2,5-bis(9,9-dihexylfluoren-2-yl)pyridine-$\kappa^2NC_{3'}$]iridium(III), Ir(HFP)$_3$, have been reported elsewhere.[26] PFO was obtained from American Dye Source, Inc. The molecular structures of PFO, PFO−F (1%), fluorenone, and Ir(HFP)$_3$ are shown in Chart 1.

(2) Measurements and Device Fabrication. For optical measurements, thin films of PFO, PFO−F(1%), and the fluorenone derivative were spin-cast from 1,2-dichloroethane solutions (1 wt %) onto fused silica substrates. The ultraviolet−visible (UV−vis) absorption spectra were obtained with a Shimadzu 2401PC UV−vis spectrophotometer. The optical densities of the PFO and PFO−F (1%) films are approximately 1.5; the optical density for the fluorenone derivative film is approximately 0.02 at the absorption maximum. PL spectra were collected with a PSI (Photon Technology International) fluorescence spectrometer with excitation at 380 nm. Both the incident beam and the detected PL were at an angle of 45° with respect to the normal to the surface of thin films.

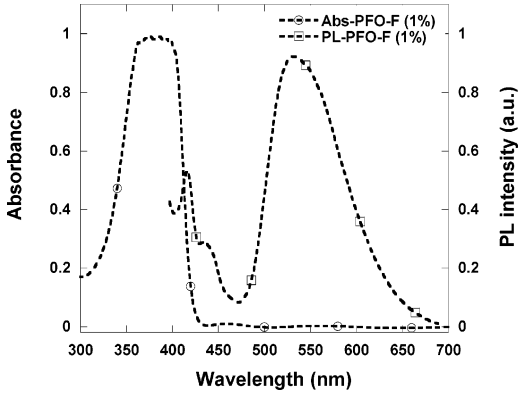

Figure 1. Absorption and PL spectra of PFO−F (1%) thin films.

Cyclic voltammetric data were obtained at room temperature using a potentiostat/galvanostat (model 263A, Princeton Applied Research). A three-electrode configuration (undivided cell) was used: the working electrode was a platinum button electrode, the counter electrode was platinum wire, and the reference electrode was Ag. The measurements were done in dichloromethane containing 0.1 M tetra-*n*-butylammonium hexafluorophosphate ($TBAPF_6$). Ferrocene was used as an internal standard and its half-wave potential was taken as +0.39 V against Ag/AgCl.[27]

For device fabrication, we employed only the single-active-layer configuration with poly(3,4-ethylenedioxythiophene):poly-(styrenesulfonic acid) (PEDOT:PSS) on indium tin oxide (ITO) as the hole-injecting bilayer electrode. The device structures are (ITO)/PEDOT:PSS/polymers/Ca/Ag (where "polymers" refers to pure PFO, pure PFO−F (1%), and the PFO:PFO−F (1%) blends, respectively) and (ITO)/PEDOT:PSS/polymer blends/Ba/Al (where polymer blends are PFO:PFO−F(1%): Ir(HFP)$_3$). The thickness of polymer films was approximately 80 nm. Details of device fabrication and testing have been reported elsewhere.[28,29] The Ca, Ba, Ag, and Al electrodes were thermally deposited at 1×10^{-7} Torr.

Results and Discussion

(1) Characterization of PFO−F (1%). The molecular weight of the PFO−F (1%) copolymer was determined by gel permeation chromatography (GPC) using polystyrenes as references. M_w and M_n were 55 000 and 32 000, respectively.

Figure 1 shows the absorption and PL spectra of PFO−F (1%) thin films. For PFO−F (1%), the absorption onsets at approximately 430 nm (2.88 eV) with a maximum absorption at 384 nm (3.23 eV), corresponding to the expected $\pi-\pi^*$ transition from the fluorene backbone. When compared to that of PFO, however, an additional weak absorption band appears at ~420 nm, which is associated with the $n-\pi^*$ transition observed in the spectroscopy of fluorenone molecules (see Figure 3). Under irradiation with light of 384 nm, the PL from PFO−F (1%) is green with a weak blue component, i.e., the same as the PL from oxidized PFO films.[25] The green emission from PFO−F (1%) films thus originates from fluorenone units within the copolymer.[30,31]

The brightness versus voltage and current density versus voltage characteristics for the devices made by PFO−F (1%) are shown in Figure 2. The PLEDs turn on at approximately 5

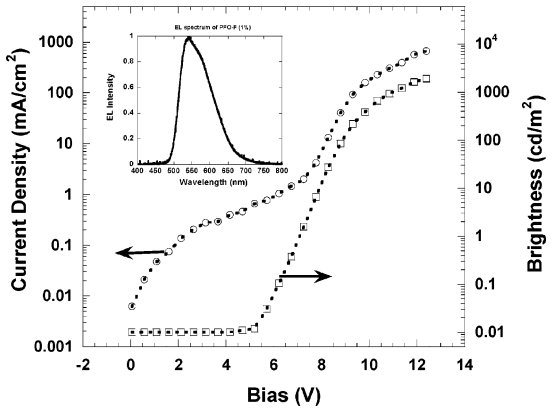

Figure 2. Luminance versus voltage and current density versus voltage characteristics for the devices made by PFO−F (1%). The inset is the electroluminescence spectrum observed from neat PFO−F (1%) PLEDs.

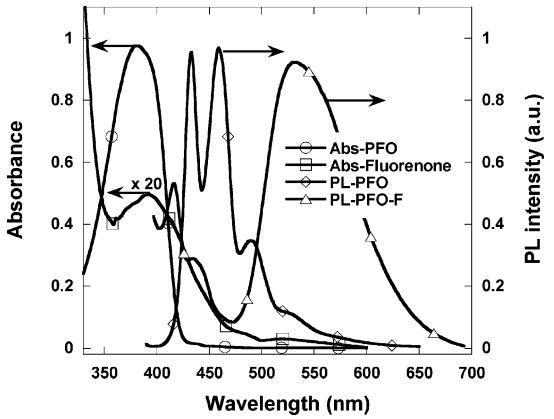

Figure 3. Normalized thin film absorption spectra of PFO and fluorenone derivative and photoluminescence spectra of PFO and PFO−F (1%).

V with a brightness approaching 2000 cd/m^2 at 12.5 V. The EL spectrum observed from PLEDs with a device configuration of (ITO)/PEDOT:PSS/PFO−F (1%)/Ca/Ag is shown in the inset of Figure 2. The EL and PL spectra are identical.

(2) Efficient Excitation Energy Transfer from PFO to the Fluorenone Defect. The absorption spectra of PFO and fluorenone thin films and the PL spectra of PFO and PFO−F (1%) thin films are shown in Figure 3. The absorption maxima for PFO and the fluorenone derivative are at 384 and 415 nm, respectively. Under irradiation with 380 nm light, the PL shows well-defined vibronic features. A weaker long-wavelength emission (∼530 nm) is also evident in the spectra. Figure 3 demonstrates that there is a good overlap between the absorption spectrum of the fluorenone derivative and the emission spectrum of PFO, implying efficient Förster energy transfer with subsequent emission from the fluorenone derivative.

To test the efficiency of Förster energy transfer, thin films of pure PFO, PFO−F(1%), and PFO with different concentrations of PFO−F(1%) were prepared and excited optically with 380 nm radiation. Normalized thin film PL spectra of PFO and PFO blended with the different concentrations of PFO−F (1%) are shown in Figure 4. The PL profile indicates two species. (1) The PL from PFO with maxima at 420 nm and 450 nm. (2) The PL from fluorenone with maximum at 530 nm. The blue emission (at 420 and 450 nm) decreases and the green emission (at 530 nm) increases as the concentration of PFO−F (1%) is increased. Direct measurements of the optical absorption at 380 nm indicate that the absorption coefficient of PFO is 20 times greater than that of the fluorenone component. Thus, for PFO−F(1%), nearly all the incident photons are absorbed by the PFO. Note that the PL lifetime of PFO and its derivatives is a few hundreds picoseconds.[32,33] These data indicate efficient Förster energy transfer from PFO to the fluorenone defects.

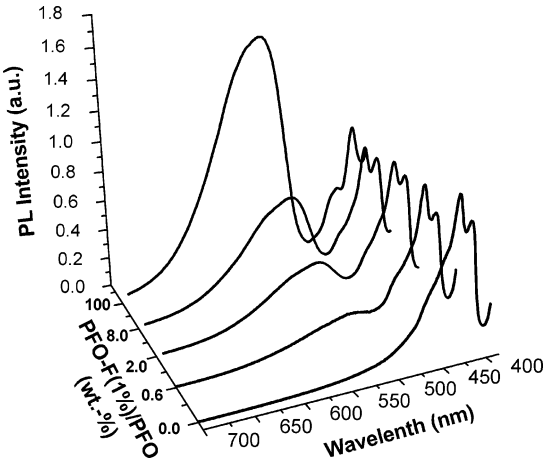

Figure 4. Normalized thin film photoluminescence spectra of PFO, PFO−F (1%), and PFO blended with different concentrations of PFO−F (1%).

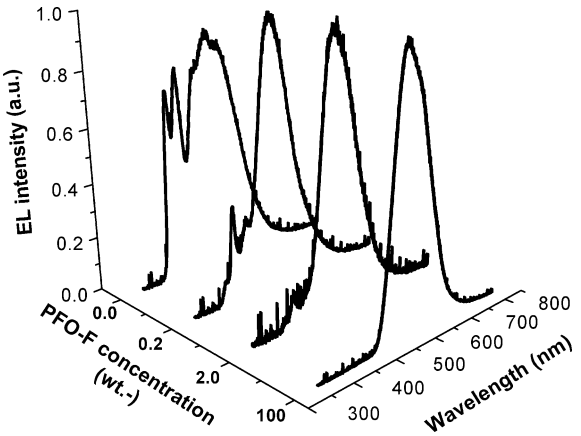

Figure 5. Normalized electroluminescence spectra of the devices made with pure PFO, PFO−F (1%), and PFO blended with different concentrations of PFO−F (1%).

Figure 5 shows the EL spectra from the devices made with pure PFO and PFO doped with different concentrations of PFO−F (1%). The green emission in the devices made with pure PFO originates from the fluorenone defects generated during device fabrication and operation.[25] The blue emission from PFO is reduced significantly as the fluorenone concentration is increased. For devices made with PFO−F (1%), the blue emission is completely quenched; the devices emitted green light. The absence of blue EL emission from the devices made with PFO−F(1%) indicates that charge carrier trapping plays an important role in the operation of light-emitting diodes (LEDs). If energy transfer were dominant in EL, the blue emission from PFO would not completely disappear and the EL spectrum should be identical to that of PL from PFO−F under optical excitation.

The highest occupied molecular orbital (HOMO) and lowest unoccupied molecular orbital (LUMO) energy levels of fluorenone are shown in Chart 2. Consistent with charge trapping, the fluorenone defects function as both a hole trap and an electron trap; the HOMO and LUMO of fluorenone fall within the $\pi-\pi^*$ gap of PFO.[34] In addition, the hole (electron) can be injected from the PEDOT:PSS (Ca) electrode directly into the HOMO (LUMO) of fluorenone because of the small energy

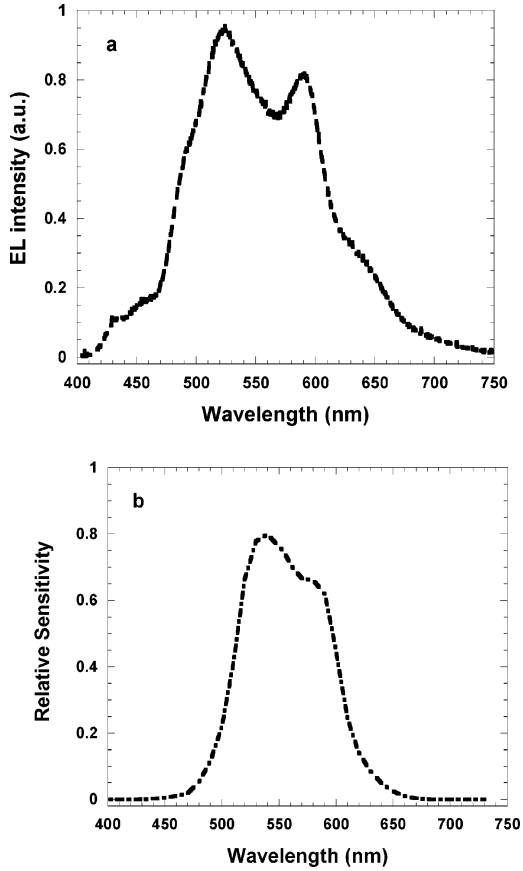

Figure 6. (a) EL spectrum obtained from white emitting electrophosphorescent PLEDs and (b) the same spectrum as in (a) but renormalized to the sensitivity of the human eye.

CHART 2: Energy Levels of PFO, PFO−F (1%) and Fluorenone Derivative

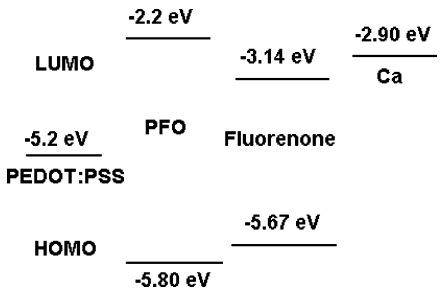

barrier between PEDOT:PSS and the HOMO (or between Ca and the LUMO) of fluorenone.

Therefore, the more pronounced green emission from PFO containing fluorenone defects results from a combination of efficient energy transfer, charge carrier trapping, and relatively easy injection (from the electrodes) of carriers into the fluorenone traps.

(3) White Electrophorescent PLEDs. Fluorenone defects cause the degradation of the blue emission to blue-green in PFs. However, fluorenone as a chemical defect added into the main chain of the polymer to form a copolymer offers the advantages of the emission from a two-component polymer blend, but it is not subject to phase separation. Therefore, the PL and EL from this copolymer is expected to be stable.

To take the advantage of built-in fluorenone defects in the PFO−F copolymer, we have fabricated white-emitting PLEDs made by PFO, PFO−F, and $Ir(HFP)_3$. Figure 6a shows the EL spectra obtained from devices with a configuration of (ITO)/PEDOT:PSS/emitting layer/Ba/Al. The emitting-layer comprises $Ir(HFP)_3$:PFO−F(1%):PFO. The same spectrum, renormalized to the sensitivity of the human eye, is shown in Figure 6b. The emission is well matched to the response of the human eye. Figure 7 shows a photo of such a device during operation.

Figure 7. Photo of white emitting device during operation. The device size was 3 cm × 3 cm.

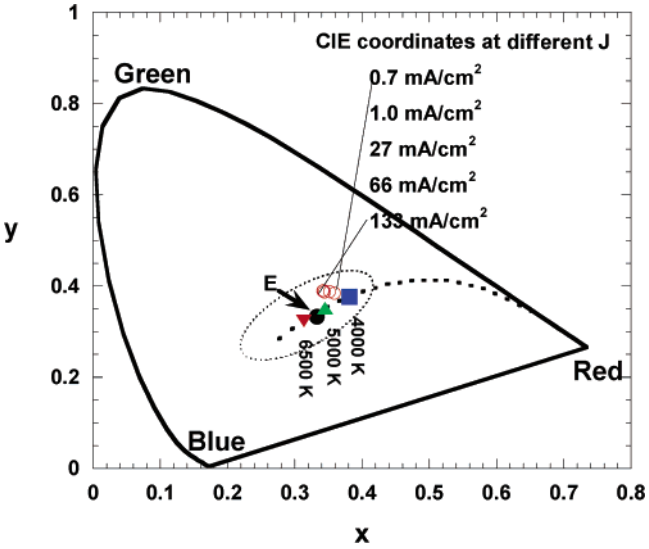

Figure 8. CIE (1931) chromaticity diagram, with coordinates corresponding to the emission from white emitting devices (○) biased at different current densities. Also shown are the equi-energy points (*E*) for pure white light (0.333, 0.333) (●) and the coordinates corresponding to color temperatures 4000 K (■), 5000 K (▲), and 6500 K (▼). The dotted line indicates different color temperatures; the dotted oval indicates the approximate area where the human eye perceives the color as white.

In the electrophosphorescent PLEDs made from the blends of $Ir(HFP)_3$:PFO−F(1%):PFO, injected holes and electrons recombine by two processes: direct recombination on the main chain (PFO) to produce blue emission in parallel with electron and hole trapping on the fluorenone units and on the $Ir(HFP)_3$ followed by radiative recombination, with green light from PFO−F (1%) and red light from the triplet excited state of $Ir(HFP)_3$.

The CIE coordinates, color temperature (CT), and color rendering index (CRI) were quantitatively evaluated from EL spectra.[35,36] Figure 8 shows the 1931 CIE chromaticity diagram, with coordinates corresponding to the emission from electrophosphorescent PLEDs: data points are shown for devices (open circles) biased at different current densities. In Figure 8, the dotted line indicates different color temperatures; the dotted oval indicates the approximate area where the human eye perceives

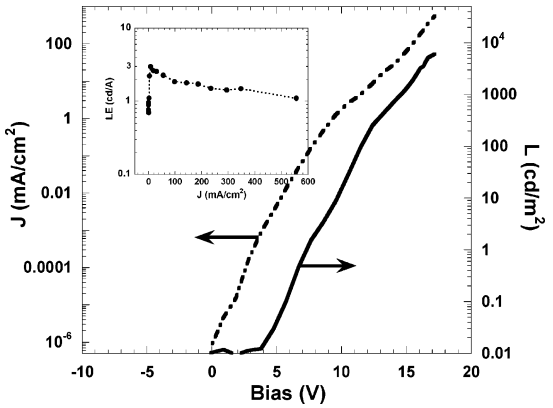

Figure 9. Luminance (L) versus applied voltage and current density (J) versus applied voltage for white light devices. The inset is the luminous efficiency (LE) versus J.

the color as white. The CIE coordinates for the $Ir(HFP)_3$:PFO−F(1%):PFO devices are (0.352, 0.388) at $J = 1$ mA/cm^2, very close to the CIE coordinates for pure white light, (0.333, 0.333). The CIE coordinates show only minor shifts at different J. The stability of the CIE coordinates as a function of the brightness and applied voltage is much better than reported previously for PLEDs/OLEDs.[10−16]

The $Ir(HFP)_3$:PFO−F(1%):PFO devices had CT $\sim$ 4600 K and CRI = 86; the CT $\sim$ 4600 K is very close to the CT of sunlight at 20° solar altitude (4700 K).[37] The CTs and CRIs are insensitive to brightness and J.

The luminance versus voltage and current density versus voltage characteristics are shown in Figure 9. The inset of Figure 9 shows the luminance efficiency as a function of J. The white emission turns on at approximately 5 V, with a luminance (L) of $L = 6100$ cd/m^2 at 17 V. A lambertian intensity profile was assumed to calculate the LE (cd/A) and the power efficiency (lm/W) with the following results: LE = 3 cd/A and $L = 255$ cd/m^2 at $J = 8.5$ mA/cm^2. The power efficiency was approximately 1 lm/W. Because the charge carriers are not balanced in these devices,[38] we anticipate that the LE and power efficiency can be enhanced by using an alternative hole injection layer.[39]

Conclusion

Poly(9,9-dioctylfluorene-*co*-fluorenone) with 1% fluorenone (PFO−F(1%)) was synthesized as a model compound to investigate the optical and electrical effects of fluorenone defects in poly(9,9-dioctylfluoren-2,7-diyl), PFO. The spectroscopic and cyclic voltammetry studies demonstrate that Förster energy transfer to and charge carrier trapping on fluorenone defects (with subsequent fluorenone emission) are responsible for the color degradation observed with the polyfluorenes.

By utilization of fluorenone defects in PFO, white electrophosphorescent PLEDs were fabricated by spin-casting polymer blends from solution containing PFO, PFO−F (1%), and $Ir(HFP)_3$. Illumination quality white light was demonstrated with stable CIE coordinates, stable color temperatures, and stable color rendering indices, all close to those of "pure" white. The simple device structure and the promise of low-cost manufacturing make these electrophosphorescent PLEDs attractive for development for solid-state lighting applications.

Acknowledgment. This work was supported by Air Force Office of Scientific Research through the MURI Center ("Polymeric Smart Skins"), Program Officer, Dr. Charles Lee. We thank Prof. G. C. Bazan and J. C. Ostrowski for providing iridium complexes.

References and Notes

(1) Heeger. A. J. *Angew. Chem., Int. Ed.* **2001**, *40*, 2591−2611; *Solid State Comm.* **1998**, *107*, 673−679; *Rev. Mod. Phys.* **2001**, *73*, 681−701.
(2) Braun, D.; Heeger, A. J. *Appl. Phys. Lett.* **1991**, *58*, 1982−1984.
(3) Yu, G.; Wang, J.; McElvain, J.; Heeger, A. J. *Adv. Mater.* **1998**, *10*, 1431−1434.
(4) Heeger, P. S.; Heeger, A. J. *Proc. Natl. Acad. Sci. U.S.A.* **1999**, *96*, 12219−12221.
(5) Dimitrakopoulos, C. D.; Mascaro, D. J. *IBM J. Res. Dev.* **2001**, *45*, 11−27.
(6) McGehee, M. D.; Heeger, A. J. *Adv. Mater.* **2000**, *12*, 1655−1668.
(7) Scherf, U.; List, E. J. W. *Adv. Mater.* **2002**, *14*, 477−487.
(8) Setayesh, S.; Marsitzky, D.; Müllen, K. *Macromolecules* **2000**, *33*, 2016−2020.
(9) Scherf, U. *J. Mater. Chem.* **1999**, *9*, 1853−1864.
(10) Kido, J.; Shionoya, H.; Nagai, K. *Appl. Phys. Lett.* **1995**, *67*, 2281−2283.
(11) Zhang, C.; Heeger, A. J. *J. Appl. Phys.* **1998**, *84*, 1579−1582.
(12) Shen, Z.; Burrows, P. E.; Bulvić, V.; Forrest, S. R.; Thompson, M. E. *Science* **1997**, *276*, 2009−2011.
(13) Hamada, Y.; Sano, T.; Fujii, H.; Nishio, Y. *Jpn. J. Appl. Phys.* **1996**, *35*, L1339−L1341.
(14) Wang, Y. Z.; Sun, R. G.; Meghdadi, F.; Leising, G.; Epstein, A. J. *Appl. Phys. Lett.* **1999**, *74*, 3613−3615.
(15) Strukelj, M.; Jordan, R. H.; Dodabalapur, A. *J. Am. Chem. Soc.* **1996**, *118*, 1213−1214.
(16) Yamamoto, T. *Prog. Polym. Sci.* **1992**, *17*, 1153−1205.
(17) Buckley, A. R.; Rahn, M. D.; Hill, J.; Cabanillas-Gonzalez, J.; Fox, A. M.; Bradley, D. D. C. *Chem. Phys. Lett.* **2001**, *339*, 331−336.
(18) Gong, X.; Ostrowski, J. C.; Bazan, G. C.; Moses, D.; Heeger, A. J.; Liu, M. S.; Jen, A. K.-Y. *Adv. Mater.* **2003**, *15*, 45−49.
(19) Lemmer, U.; Heun, S.; Mahrt, R. F.; Scherf, U.; Hopmeier, M.; Siegner, U.; Göbel, E. O.; Müllen, K.; Bässler, H. *Chem. Phys. Lett.* **1995**, *240*, 373−378.
(20) Bliznyuk, V. N.; Carter, S.A; Scott, J. C.; Klärner, G.; Miller, R. D.; Miller, D. C. *Macromolecules* **1999**, *32*, 361−369.
(21) List, E. J. W.; Guentner, R.; de Freitas, P. S.; Scherf, U. *Adv. Mater.* **2002**, *14*, 374−378.
(22) Romaner, L.; Poganisch, A.; Scandiucci de Freitas, P.; Scherf, U.; Gaal, M.; Zojer, E.; List, E. J. W. *Adv. Funct. Mater* **2003**, *13*, 597−601.
(23) Gaal, M.; List, E. J. W.; Scherf, U. *Marcomolecules* **2003**, *36*, 4236−4237.
(24) List, E. J. W.; Gaa, M.; Guentner, R.; Scandiucci de Freitas, P.; Scherf, U. *Synth. Met.* **2003**, *139*, 759−763.
(25) Gong, X.; Iyer, P. K.; Moses, D.; Bazan, G. C.; Heeger, A. J. *Adv. Funct. Mater.* **2003**, *13*, 325−330.
(26) Ostrowski, J. C.; Robinson, M. R.; Heeger, A. J.; Bazan, G. C. *Chem. Commun.* **2002**, *7*, 784−785.
(27) Li, Y. F.; Cao, Y.; Gao, J.; Wang, D.; Yu, G.; Heeger, A. J. *Synth. Met* **1999**, *99*, 243−248.
(28) Gong, X.; Ostrowski, J. C.; Robinson, M. R.; Moses, D.; Bazan, G. C.; Heeger, A. J. *Adv. Mater.* **2002**, *14*, 581−585.
(29) Gong, X.; Ostrowski, J. C.; Bazan, G. C.; Moses, D.; Heeger, A. J. *Adv. Func. Mater.* **2003**, *13*, 439−444.
(30) Arathi Rani, S.; Sobhanadri, J.; Prasada Rao, T. A. *J. Photochem. Photobiol. A: Chem.* **1996**, *94*, 1−5.
(31) Lee, J. I.; Klaerner, G.; Miller, R. D. *Chem. Mater.* **1999**, *11*, 1083−1088.
(32) Lyons, B. P.; Wong, K. S.; Monkman, A. P. *J. Appl. Phys.* **2003**, *118*, 4707−4711.
(33) Buckley, A. R.; Rahn, M. D.; Hill, J.; Cabanillas-Gonzalez, J.; Fox, A. M.; Bradley D. D. C. *Chem. Phys. Lett.* **2001**, *339*, 331−336.
(34) Shaheen, S. E.; Kippelen, B.; Peyghambarian, N.; Wang, J. F.; Anderson, J. D.; Mash, E. A.; Lee, P. A.; Armstrong, N. R.; Kawabe, Y. *J. Appl. Phys.* **1999**, *85*, 7939−7945.
(35) Wyszelki, G.; Stiles, W. S. *Color Science*, 2nd ed.; Wiley: New York, 1982; pp. 117−232.
(36) Judd, D. B.; WyszeckI, G. *Color in Business, Science and Industry*, 3rd ed.; John Wiley & Sons: 1975; pp 91−388.
(37) Hunt, R. W. G. *Measuring Color*, 2nd ed.; Ellis Horwood: Chichester, U.K., 1991; pp 38−109.
(38) Gong, X.; Ma, W. L.; Ostrowski, J. C.; Bechgaard, K.; Bazan, G. C.; Moses, D.; Heeger, A. J.; Xiao, S. *Adv. Func. Mater.* **2004**, *14*, 393−397.
(39) Gong, X.; Moses, D.; Heeger, A. J.; Liu, S.; Jen, A. K.-Y. *Appl. Phys. Lett.* **2003**, *83*, 183−185.